Force-position modeling and control of a two robots based platform for automated pick-and-place task using H_∞ technique

Mourad Benoussaad [*] **Alejandro De Lucio Rangel** [*,**]
Gerardo I. Perez-Soto [***] **Karla A. Camarillo-Gómez** [**]
Micky Rakotondrabe [*]

[*] *LGP laboratory, ENIT-INPT, University of Toulouse, Tarbes France.*
[**] *Mech Eng dept, Instituto Tecnológico de Celaya, GTO Mexico.*
[***] *Ingeniería faculdad, Universidad Autónoma de Querétaro, Mexico*

(corresponding author: mrakoton@enit.fr)

Abstract: This paper proposes the modeling and the control of two robots that co-manipulate an object. In the studied strategy, one robot is controlled on position whilst the other on force which will permit precise positioning of the object while mastering the manipulation force. On the other hand, the object is considered deformable which renders the manipulation task very challenging. For that, we propose to model the object deformation and include it in the controllers design. The robust H_∞ technique is proposed to design the force and the position controllers such that prescribed performances be obtained and disturbance effects due to the object be rejected. An automated pick-and-place task is simulated which validates the interest of the proposed force-position control techniques.

Keywords: Force-position control, Robotics, Pick-And-Place task, H_∞ technique.

1. INTRODUCTION

One common task in industrial production environments is pick-and-place, which consists of taking an object from one location and placing it in another one. Such task is still applied in Industry 4.0 where handled objects may be light or heavy, rigid or flexible/deformable. Robotic manipulation of deformable/flexible objects becomes very challenging when highly precise tasks have to be done or when the objects dimensions are large. For the former, the traditional use of passive compliance placed as interface between the robot' end-effector and the manipuated object is not anymore sufficient to ensure the precision of the tasks as the deformation itself introduces uncertainties in the positioning. For the second case, manipulation of large or long deformable/flexible objects which require two manipulators is typified by additional uncontrollable degrees of freedom (the deformation itself) which drastically compromise the stability of the tasks [1]. The use of effective controllers for the robots is thus unavoidable.

Within the ECOSYSPRO project at LGP laboratory, one of the targets consists in automatizing and robotizing pick-and-place tasks that will be useful for an Industry 4.0 context. For that, two robots are used to pick heavy bags filled of seeds (rices, corns...) from one place and transport each of them to another place where a human operator will partly empty or fill. During the emptying/filling task, the two robots should keep and maintain the bag firmly at its position. The bags filled of seeds are considered as large and deformable objects which definitely render their robotic manipulation very challenging. This paper deals with the modeling and control of the used two robots for pick-transport-and-place manipulation tasks.

Two robotic arms based manipulation permits to adapt to different sizes and shapes of objects and to control both the position and the force in an active way. Furthermore, if an additional task such as machining is planned, it is likely more robust to keep the object with two arms than one. In this context, several previous research investigated the robotic dual-arm manipulation [2]-[3] and its co-manipulation with a human partner [4]. In these works, the control is commonly based on combination of force and position to handle a rigid or a deformable objects. Regarding the control of two independent robots for manipulation, vision system has been used to drive them and to characterize the manipulated objects [5]-[7]. Vision based control of collaborative robots is interesting as it brings external and general information on the systems and on the task. However, local states on the collaboration, such as the manipulation force, can not be observed precisely. Moreover, visual feedback cannot provide full information if the object exhibits complex shape, or if there are obstacles between the cameras and the robots. Hence, contact-based measurement for feedback control is seen as a promising approach to complement the visual feedback. In [8], the grasping force was controlled during manipulation tasks, however the position was not. In [9], both the force and the position were controlled but the object was not flexible nor deformable. In [10], force-position control of millimeters sized deformable objects

⋆ This work is partially funded by the national-regional CPER ECOSYSPRO project.

was considered using interval techniques [11], also used for robust design of the actuators used [12]. These works demonstrated that the manipulated objects characteristics affect the force control in a drastic way if not accounted for.

This paper deals with the simultaneous force-position control of two independent robots manipulating an object as part of the ECOSYSPRO project. The manipulated object is large and deformable and represents a bag of seeds with variable properties (mass, stiffness...) according if it is fully filled or not which therefore can affect the feedback controlled system performances. Moreover, the interaction between the two robots through the manipulated objects can also drastically introduce unstability of the tasks if not considered appropriately. We propose to control independently the two robots, one for position and the other for force. For the position control, the interaction through the object is accounted as external disturbance whilst a H_∞ controller is designed. For the force control, we propose first an internal loop to cancel the object properties effects. Then an outer H_∞ force controller is designed. The proposed H_∞ techniques permit to ensure the performances despite the interaction between the two robots. In the project, the force is measured thanks to a piezoelectric sensor using the self-sensing technique [13].

The paper is organized as follows. Section-II presents the two robots based platform and the governing equation useful for further modeling. The modeling and the control of the position is afterwards detailed in section-III while those of the force in section-IV, along with simulation are presented for validation. Section-V presents an example of pick-and-place task simulation and section-VI gives the concluding remarks and some perspectives.

2. PRESENTATION OF THE PLATFORM AND GOVERNING EQUATIONS

2.1 Presentation of the platform

The robotic platform used is composed of two linear robots that combine piezoelectric actuation and standard DC Motors. The piezoelectric actuation also permits the force measurement thanks to piezoelectric properties. Fig 1 presents a CAD image of the platform that includes the two robots and the manipulated object and its representation for further modeling.

2.2 Governing models

The two robots are the same and are based on electromechanical actuation driven by voltages. The behavior of each of them is:

$$x_i = \alpha_i D_i(s) u_i - \beta_i D_i(s) F_i \tag{1}$$

where x_i is the linear displacement, u_i is the driving voltage, and F_i is a force applied by the external to the robot. Coefficients α_i and β_i are the electromechanical constant and the compliance constant respectively. On the other hand, $D_i(s)$ is a transfer function representing the dynamics of the robot. Subscript i stands for l (left) or r (right). The numerical values are:

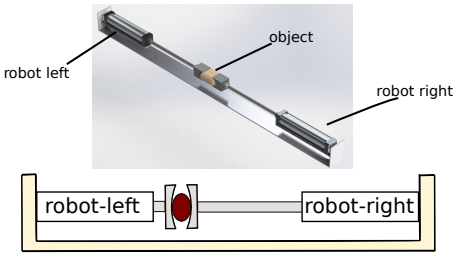

Fig. 1. CAD image of the robotic platform (up). Representation for modeling (down).

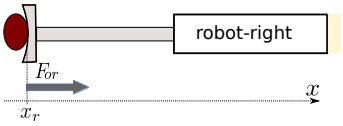

Fig. 2. Representation for the position modeling.

$$\begin{cases} \alpha_i = 0.02 \left[\dfrac{m}{V}\right] ; \ \beta_i = 0.02 \left[\dfrac{m}{N}\right] \\ D_i(s) = \dfrac{0.044\,(s+12)\,(s+3)}{(s+2)\,(s+0.8)\,(s^2+0.4s+1)} \end{cases} \tag{2}$$

When the two robots manipulate an object, the behavior of each of them will affect the other through it. This mutual effect can be seen as a disturbance for each robot. In the sequel, one robot will be controlled for the positioning whilst the other will be controlled on force by delicately considering this disturbance or effect. Without loss of generality, we choose the right robot for the position control and the left robot for the force.

3. POSITION MODELING AND H_∞ CONTROL

This section presents the object position modeling and the control by using the right robot, see Fig 2.

3.1 Modeling

Taking the contact point between robot and object as the latter's position, the model is obtained from Eq.(1) as:

$$x_r = \alpha_r D_r(s) u_r + \beta_r D_r(s) F_{or} \tag{3}$$

where x_r is the right robot (and thus the object's) position, F_{or} is the force applied by the object to the robot, and u_r is its driving voltage. Taking the force as disturbance, Eq.(4) can be rewritten to derive the final position model:

$$x_r = G_r(s) u_r + d_r \tag{4}$$

in which we have the disturbance $d_r = \beta_r D_r(s) F_{or}$, and the system $G_r(s) = \alpha_r D_r(s) u_r$.

3.2 Specifications for the closed-loop

Let Fig 3(a) be the closed-loop diagram, in which x_{rd} is the desired or reference position and e_r is the tracking error. The target is to calculate the controller $C_r(s)$ such that some prescribed performances specifications be satisfied. The standard H_∞ technique is proposed for the controller calculation in order to ensure robustness of these performances against the disturbance and against

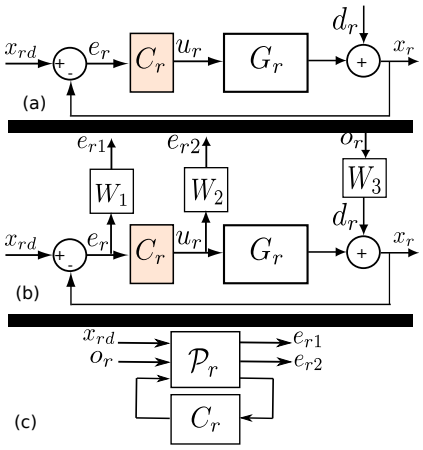

Fig. 3. Block diagram. (a): the closed-loop. (b): the augmented closed-loop. (c): the standard form.

possible model uncertainties. On the basis of the expected application, the following specifications are given.

Tracking performances: we want that the closed-loop have a settling time of $3s$, a static error of 1% and zero overshoot when a step reference x_{rd} is applied.

Voltage saturation: we want that a step reference at its maximal range $(2m)$ yields voltage limited to $200V$.

Disturbance rejection: we want that a step disturbance force d_r be rejected quickly, without overshoot, and with a static error of $\frac{0.001m}{1N}$.

3.3 Standard form and H_∞ problem

In standard H_∞ technique, the prescribed specifications are exploited explicitely. In our case, three weightings $W_1(s)$, $W_2(s)$ and $W_3(s)$ are introduced for the the tracking performance, the input saturation and the disturbance rejection respectively following the augmented closed-loop described in Fig 3(b). In the diagram, e_{r1} and e_{r2} are called weighted outputs and o_r is the new input. Note that this augmented closed-loop is only used for the controller synthesis and not for the implementation. From the numerical values of the above specifications, we propose the gains:

$$\frac{1}{W_1} = \frac{s+0.01}{s+1}; \quad \frac{1}{W_2} = \frac{200[V]}{2[m]}; \quad \frac{1}{W_1 W_3} = \frac{s+0.01}{0.9s+1} \tag{5}$$

with $\frac{1}{W_1} = \frac{e_{r1}}{x_{rd}}$, $\frac{1}{W_2} = \frac{e_{r2}}{x_{rd}}$ and $\frac{1}{W_1 W_3} = \frac{e_{r1}}{d_r}$. To further apply the standard H_∞ synthesis, the augmented closed loop of Fig 3(b) is transformed into standard form displayed in Fig 3(c) where $\mathcal{P}_r(s)$ rassembles the system $G_r(s)$ and the weightings $W_i(s)$. Using the standard H_∞ approach [14], our problem consists in seeking for an optimal (minimal) value of $\gamma_r > 0$ and an optimal controller $C_r(s)$ such that:

$$\left\| L_{lower}\left(\mathcal{P}_r(s), C_r(s)\right) \right\|_\infty < \gamma_r \tag{6}$$

where $L_{lower}\left(\mathcal{P}_r(s), C_r(s)\right)$ is the lower linear fractional transformation defined by:

$$\begin{pmatrix} e_{r1} \\ e_{r2} \end{pmatrix} = L_{lower}\left(\mathrm{P}_r(s), C_r(s)\right) \begin{pmatrix} x_{rd} \\ o_r \end{pmatrix} \tag{7}$$

3.4 Problem reformulation

In order to rewrite condition in Ineq.(6) as explicit function of the controller to be calculated, of the system and of the weigthings, let us compute $L_{lower}\left(\mathcal{P}_r(s), C_r(s)\right)$. To this aim, Fig 3(b) permits to have:

$$\begin{cases} e_{r1} = W_1 S_r x_{rd} - W_1 S_r W_3 o_r \\ e_{r2} = W_2 C_r S_r x_{rd} - W_2 C_r S_r W_3 o_r \end{cases} \tag{8}$$

where $S_r = \frac{C_r G_r}{(1+C_r G_r)}$ is the sensitivity function.

Considering Eq.(8), Ineq.(7) and Eq.(6), the H_∞ problem becomes in seeking $C_r(s)$ such that:

$$\begin{pmatrix} \|W_1 S_r\|_\infty < \gamma_r & \|W_1 S_r W_3\|_\infty < \gamma_r \\ \|W_2 C_r S_r\|_\infty < \gamma_r & \|W_2 C_r S_r W_3\|_\infty < \gamma_r \end{pmatrix} \tag{9}$$

which is satisfied if there exists a controller $C_r(s)$ s.t.:

$$\begin{pmatrix} |S_r| < \gamma_r \left|\frac{1}{W_1}\right| & |S_r| < \gamma_r \left|\frac{1}{W_1 W_3}\right| \\ |C_r S_r| < \gamma_r \left|\frac{1}{W_2}\right| & |C_r S_r| < \gamma_r \left|\frac{1}{W_2 W_3}\right| \end{pmatrix} \tag{10}$$

3.5 Controller derivation

By applying the Doyle-Glover algorithm [15] to the problem in Ineq.(10), we obtain an optimal performance level $\gamma_r = 2.7$ and an optimal controller $C_r(s)$ of order 7. Such order could be high to the implementation, thus we reduced the controller with the balanced realization technique [16], which yielded an order of 4, see Eq.(11). Below an order of 4, the closed-loop loses performances.

$$C_r(s) = \frac{-0.74\left(s - 2.5\times10^4\right)(s+0.77)\left(s^2+0.4s+0.99\right)}{(s+143)(s+0.01)\left(s^2+2.44s+3.58\right)} \tag{11}$$

3.6 Simulation results

The controller Eq.(11) was implemented in Matlab using Fig 3(b). A step reference position of $x_d = 1m$ is applied whilst the initial position of the object was $0m$. Fig 4 (...) displays the response of the closed-loop. In the figure, the behavior of the gain $(1 - \frac{1}{W_1})$ (desired closed-loop) is also displayed in (- - -), as well as the scaled response of the robot without controller in (—). The result clearly indicates that the closed-loop exhibits very good performances in comparison to the initial robot. Furthermore, the desired settling time $(3s)$ as well as the static error (1%) fit with the specifications, whilst the overshoot is negligible. Finally, Fig 5 gives the response of the closed-loop when a step force disturbance of $0.5N$ is applied at time $t = 15s$ and demonstrates its rejection in a convenient manner.

4. FORCE MODELING AND H_∞ CONTROL

To perform the force modeling, we propose to model the deformable object with a mass-damper-spring system which is sufficient for manipulator-object interaction analysis [17]. Hence Fig 6 depicts the left robot in contact with the object, the latter being blocked by the right robot at its other extremity. In the figure, m_o, k_o and c_o are the effective mass, the stiffness and the damping coefficient of the object during deformation.

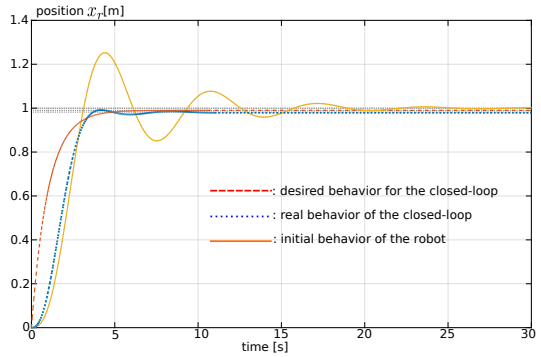

Fig. 4. Simulation result: behavior comparison.

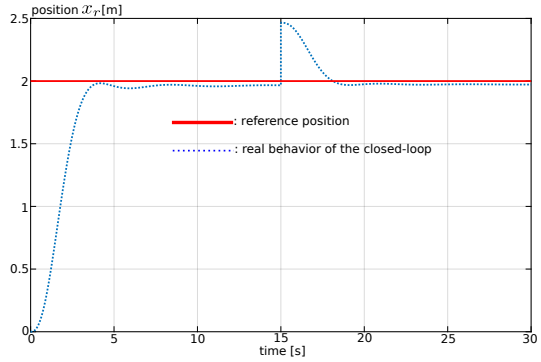

Fig. 5. Simulation result: step response

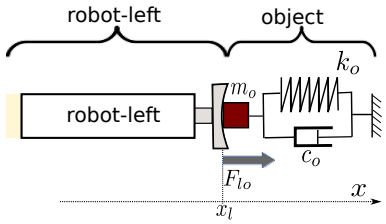

Fig. 6. Representation for the force modeling.

4.1 Modeling

Derivation of the model Using the robot model in Eq.(1) and the object deformation model, we have:

$$\begin{cases} x_l = \alpha_l D_l(s) u_l - \beta_l D_l(s) F_{lo} \\ x_l = \beta_o D_o(s) F_{lo} \end{cases} \tag{12}$$

where: $D_o(s) = \frac{1}{\frac{m_o}{k_o}s^2 + \frac{c_o}{k_o}s + 1}$ and $\beta_o = \frac{1}{k_o}$. The dynamics $D_o(s)$ and $D_l(s)$ are normalized, i.e. $D_o(0) = 1$ and $D_l(0) = 1$. We also have F_{lo} as the force applied by the left robot to the object, called manipulation force.

From Eq.(12), we obtain the force model as:

$$\frac{F_{lo}(s)}{u_l(s)} = \frac{\alpha_l D_l(s)}{(\beta_o D_o(s) + \beta_l D_l(s))} \tag{13}$$

Causality verification First let us check the causality of Eq.(12) since the dynamics D_o and D_l are in the denominator. Decomposing $D_l(s)$ and $D_o(s)$ into numerators and denominators polynomials such that: $D_l(s) = \frac{D_{lnum}(s)}{D_{lden}(s)}$ and $D_o(s) = \frac{D_{onum}(s)}{D_{oden}(s)}$, Eq.(13) becomes:

$$\frac{F_{lo}(s)}{u_l(s)} = \frac{\alpha_l D_{lnum} D_{oden}}{(\beta_o D_{onum} D_{lden} + \beta_l D_{lnum} D_{oden})} \tag{14}$$

Considering $\partial(\cdot)$ as the degree of a polynomial, the force model in Eq.(14) and thus that of Eq.(13) is always causal because the following statement is always true:

$$\partial(\alpha_l D_{lnum} D_{oden}) \leq \partial(\beta_o D_{onum} D_{lden} + \beta_l D_{lnum} D_{oden}) \tag{15}$$

Model rearrangement As we can observe from Eq.(13), the force model depends on the object characteristics D_o and β_o. This dependance will require a computation of the feedback controller (based on H_∞ in our case) each time the manipulated object is changed, which is very heavy and time consuming. Therefore we suggest to compensate for the objects characteristics in the model and afterwards apply the feedback controller design on the basis of the robot model only. To this aim, let us first rewrite the model in Eq.(13). After development and adding and substracting F_{lo}, we have:

$$\beta_o D_o F_{lo} + \beta_l D_l F_{lo} + F_{lo} - F_{lo} = \alpha_l D_l u_l \tag{16}$$

thus:

$$F_{lo} = \alpha_l D_l \left[u_l - \frac{1}{\alpha_l D_l} (\beta_o D_o + \beta_l D_l - 1) F_{lo} \right] \tag{17}$$

Because we employ the inverse of the dynamics $D_l(s)$ in the rearranged model of Eq.(17), a condition to make the latter usable is that $D_l(s)$ should be bi-causal (i.e. both $D_l(s)$ and its inverse should be causal). A bicausal model equivalent to $D_l(s)$ given in Eq.(2) is therefore proposed in Eq.(18) for the denominator of Eq.(17) purpose when the latter will be used as compensator. Eq.(18) is equivalent to Eq.(2) in the sense that they exhibit the same Bode magnitude in a frequency range of interest.

$$D_{lm}(s) = \frac{0.044\,(s+12)\,(s+3)\left(\frac{1}{20}s+1\right)\left(\frac{1}{22}s+1\right)}{(s+2)\,(s+0.8)\,(s^2+0.4s+1)} \tag{18}$$

The model in Eq.(17) can be represented by the diagram in Fig 7(a) where all the object characteristics are rassembled in the negative feedback.

Positive feedback compensation and new model The negative feedback in the diagram of Fig 7(a) can be compensated for by using a positive feedback as depicted in Fig 7(b). As a result, we obtain an equivalent diagram as depicted in Fig 7(c) where the object characteristics does not appear anymore but a new driving input v_l is introduced. Hence, the new model that links the output force F_{lo} and the new input and that will be used for controller synthesis is:

$$F_{lo} = \alpha_l D_l(s) v_l = G_l(s) v_l \tag{19}$$

4.2 Specifications for the closed-loop

Fig 7(d) depicts the closed-loop where F_d is the desired or reference force and e_l is the tracking error. Similarly to the position control, we impose prescribed specifications for the closed-loop. They are as follows.

Tracking performances: we want that the closed-loop have a settling time of $0.5s$ (which is much more rapid than for the position control to ensure highly reactive force

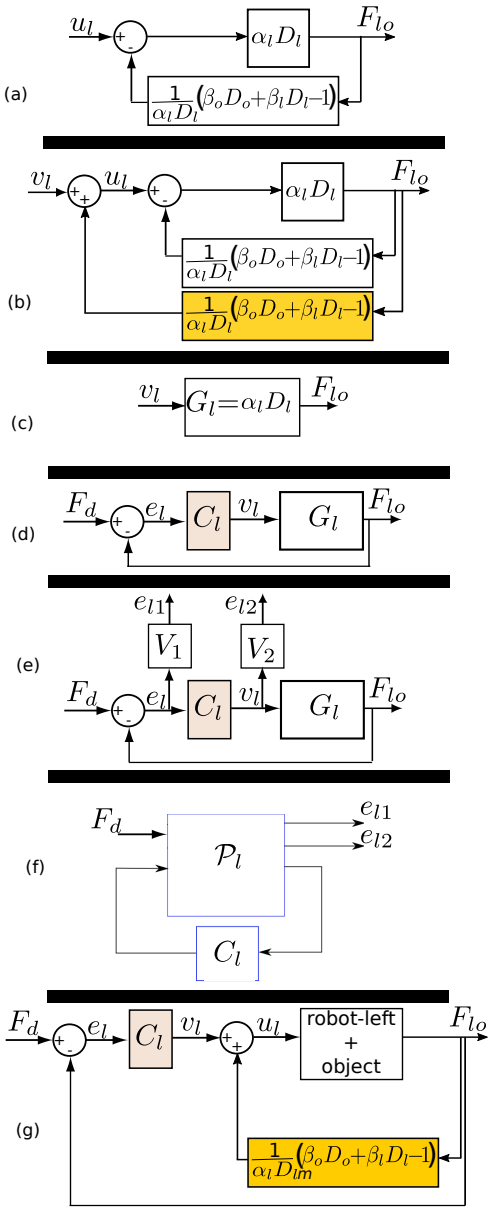

Fig. 7. Block diagram. (a): the rearranged model. (b): the rearranged model with positive feedback compensation. (c): equivalent for the new model. (d): closed-loop with the new model. (e): augmented closed-loop. (f): standard form. (g): implementation scheme.

tracking when the object is moved), a static error of 1% and zero overshoot when a step reference is applied.

Voltage saturation: we want that the voltage v_l be saturated at $200V$ for a step reference with maximal range of $F_d = 2N$.

From the specifications, weightings V_1 and V_2 are introduced for the tracking performances and voltage saturation respectively with which we create the augmented closed-loop of Fig 7(e). Using the numerical values of the specifications above, we propose the following gains:

$$\frac{1}{V_1} = \frac{0.1667s + 0.01}{0.1667s + 1}; \; \frac{1}{V_2} = \frac{200[V]}{2[N]} = 100 \left[\frac{V}{N}\right] \tag{20}$$

where $\frac{1}{V_1} = \frac{e_{l1}}{F_d}$ and $\frac{1}{V_2} = \frac{e_{l2}}{F_d}$, and e_{li} are the weighted outputs.

4.3 Derivation of the standard form and H_∞ problem

Fig 7(f) is the standard form related to Fig 7(e) in which $\mathcal{P}_l(s)$ includes the system G_l and the weightings. Hence, again, using the standard H_∞ problem [14], our problem consists in seeking for an optimal value $\gamma_l > 0$ and an optimal controller $C_l(s)$ such that the following inequality holds:

$$\left\| L_{lower}\left(\mathcal{P}_l(s), C_l(s)\right)\right\|_\infty < \gamma_r \tag{21}$$

where $L_{lower}\left(\mathcal{P}_l(s), C_l(s)\right)$ is the lower linear fractional transformation between the augmented system $\mathcal{P}_l$ and the controller C_l, and is defined by:

$$\begin{pmatrix} e_{l1} \\ e_{l2} \end{pmatrix} = L_{lower}\left(\mathcal{P}_l(s), C_l(s)\right) F_d \tag{22}$$

4.4 Problem reformulation

To reformulate the problem in Ineq.(21) as explicit function of C_l, of G_l and of the weightings, let us first compute $L_{lower}\left(\mathcal{P}_l(s), C_l(s)\right)$. From Fig 7(e), we have:

$$\begin{cases} e_{l1} = V_1 S_l F_d \\ e_{l2} = V_2 C_l S_l F_d \end{cases} \tag{23}$$

where $S_l = \frac{C_l G_l}{(1 + C_l G_l)}$ is the sensitivity function.

Hence, the problem in Ineq.(21) becomes in seeking for C_l s.t.:

$$\begin{pmatrix} \|V_1 S_l\|_\infty < \gamma_l \\ \|V_2 C_l S_l\|_\infty < \gamma_l \end{pmatrix} \tag{24}$$

which is satisfied if there exists a controller C_l s.t.:

$$\begin{pmatrix} |S_l| < \gamma_l \left|\frac{1}{V_1}\right| \\ |C_l S_l| < \gamma_l \left|\frac{1}{V_2}\right| \end{pmatrix} \tag{25}$$

Note that D_l in Eq.(2) is used for the H_∞ feedback design and D_{lm} in Eq.(18) is only used for the positive feedback compensation described in Fig 7(b).

4.5 Controller derivation

Using the Doyle-Glover algorithm, we obtained a $\gamma_l = 0.96$ and a controller of order 5 which was reduced to 4 when applying the equilibrium reduction technique:

$$C_l(s) = \frac{24.9\,(s + 68)\,(s + 1.79)\,\left(s^2 + 0.3s + 7.45\right)}{(s + 117)\,(s + 12)\,(s + 2.26)\,(s + 0.06)} \tag{26}$$

4.6 Simulation result

The final control implemented for the force is composed of the positive feedback compensation and of the H_∞ controller C_l, see Fig 7(g). The step response of the closed-loop is displayed in Fig 8 (...) when a desired force $F_d = 1N$ is applied. In the meantime, the scaled step response of the system without control is also displayed in Fig 8 (—), as

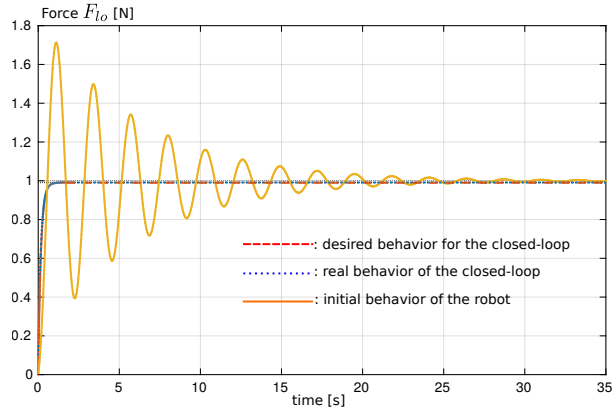

Fig. 8. Simulation result: behavior comparison.

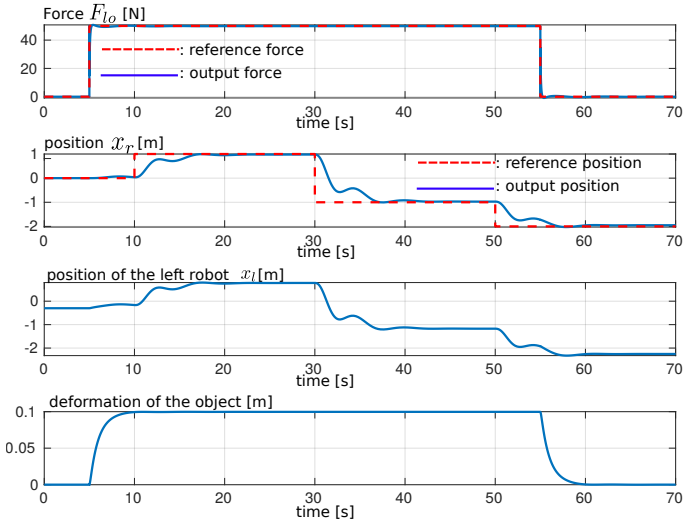

Fig. 9. Simulation result: automated pick and place task.

well as the response of specification $(1 - \frac{1}{V_1})$ in Fig 8 (- - -). It clearly appears that the badly damped oscillations of the robot-object are completely removed when using the proposed controller. Moreover, the specified performances are satisfied: settling time of $\approx 0.5s$ and no overshoot.

5. AUTOMATED PICK-AND-PLACE TASKS

To demonstrate the effectiveness of the force-position control in performing tasks, we simulated the two controlled robots in a pick-and-place context. Fig 9(a) and (b) show the resulting manipulation force and the position. At time $t = 5s$, a force reference $F_d = 50N$ is applied to the left robot in order to press the object for its picking. Then a series of position references are applied to the right robot: $x_{rd} = 1m$ at $t = 10s$, $-1m$ at $t = 30s$, and $-2m$ at $t = 50s$. Finally, the object is released at $t = 55s$ by applying a reference force of $0N$. Fig 9(c) and (d) show the position of the left robot (controlled on force) and the deformation of the object respectively during the task, which show the stability of the latter although the coupling between the two robots and the presence of deformable object.

6. CONCLUSION AND PERSPECTIVES

This paper presented the modeling and force-position control of two robots manipulating a deformable object. Whilst the object's deformation was modeled with a mass-spring-damper system, H_∞ controllers were proposed for the position and force to ensure prescribed specifications. Furthermore, a compensator was proposed to obtain a force model independent from the object properties. Simulations demonstrated the efficiency of the proposed force-position control while manipulating object during a pick-and-place task. Future work includes the application of the approach to a real benchmark.

REFERENCES

[1] Y. C. Hou, et al., "A review on modeling of flexible deformable object for dexterous robotic manipulation", Int Journal of Advanced Robotic Systems, 16(3), 2019.

[2] A. Delgado et al., "Tactile control based on Gaussian images and its application in bi-manual manipulation of deformable objects", Rob. Auton. Syst., 94, 2017.

[3] C. Jiao et al., "Adaptive Hybrid Impedance Control for A Dual-arm Robot Manipulating An Unknown Object", IEEE IECON, 2754–2759, 2020.

[4] M. Gienger et al., "Human-Robot Cooperative Object Manipulation with Contact Changes", IEEE Int Conf on Intelligent Robots and Systems, 1354–1360, 2018.

[5] T. B. Jørgensen et al., "An adaptive robotic system for doing pick and place operations with deformable objects", J. of Intelligent & Robot. Syst., 94(1), 2019.

[6] A. Petit et al., "Tracking elastic deformable objects with an RGB-D sensor for a pizza chef robot", Robotics and Autonomous Systems, 88, 187-201, 2017.

[7] J. Sanchez et al., "Robotic manipulation and sensing of deformable objects in domestic and industrial applications: a survey", International Journal of Robotics Research, 37(7), 688-716 2018.

[8] M. Kaboli et al., "Tactile-based manipulation of deformable objects with dynamic center of mass", IEEE Int Conf on Humanoid Robots, 752-757, 2016.

[9] S. Chiaverini and L. Sciavicco, "The parallel approach to force/position control of robotic manipulators", IEEE Trans on Rob and Autom, 9(4), 361-373, 1993.

[10] S. Khadraoui et al., "Interval force/position modeling and control of a microgripper composed of two collaborative piezoelectric actuators and its automation", Int Journ of Control, Autom and Systems, 12(2), 2014.

[11] M. Rakotondrabe, "Performances inclusion for stable interval systems", ACC, 4367-4372, CA USA, 2011.

[12] S. Khadraoui et al., "Optimal design of piezoelectric cantilevered actuators with guaranteed performances by using interval techniques", IEEE Trans Mechatronics, 19(5), 2013.

[13] M. Rakotondrabe, "Combining self-sensing with an Unkown-Input-Observer to estimate the displacement, the force and the state in piezoelectric cantilevered actuator", ACC, 4523-4530, 2013.

[14] G. J. Balas et al., "μ-analysis and synthesis toolbox", The Mathworks User's Guide-3, 2001.

[15] J. C. Doyle et al., 'State-space solutions to standard H_2 and H_∞ control problems', IEEE Trans on Automatic Control, 34(8), 831-846, 1989.

[16] B. C. Moore, 'Principal component analysis in linear systems: controllability, observability and model reduction', IEEE Trans on Automatic Control, 26(1), 1981.

[17] S. D. Eppinger and W. P. Seering, "On dynamic models of robot force control", IEEE ICRA, 1986.